12-6-2013

Stability and Entanglement in an Optomechanical System

Matthew Schumacher

Stability and Entanglement in an Optomechanical System

by

Matthew Schumacher

A Thesis Submitted in Partial Fulfillment of the Requirements
for the Degree of Master of Science in Applied Mathematics
School of Mathematical Sciences, College of Science

Rochester Institute of Technology
Rochester, NY
December 06, 2013

Committee Approval:

R·I·T
College of
SCIENCE

Mishkatul Bhattacharya, Ph.D. Date

School of Physics and Astronomy

Thesis Advisor

Anthony Harkin, Ph.D. Date

School of Mathematical Sciences

Committee Member

David Ross, Ph.D. Date

School of Mathematical Sciences

Committee Member

Nathan Cahill, D.Phil. Date

School of Mathematical Sciences

Director of Graduate Programs

Abstract

Optomechanical systems are currently of great interest as they lie at the boundary between quantum and classical mechanics, promising fundamental insights as well as new technologies. The practical operation of an optomechanical system requires that it satisfy the criteria of mechanical stability. Further, for quantum applications, it is important to characterize the degree of nonclassical correlation present between the mechanical and optical subsystems. In this study, we analyze the stability and entanglement in an optomechanical system where couplings linear as well as quadratic in the mechanical displacement are present simultaneously. Such systems can be realized experimentally. Our analysis of the optomechanical system is accomplished by inspecting the equations of motion that characterize the system. By analyzing the steady state of the system, we find a stability diagram which differs dramatically from the case of pure linear coupling which has been studied earlier. Specifically, we find generally a major loss of stability and a disconnection of the stability diagram when a quadratic coupling is introduced. We derive and state analytically in this thesis the stability criteria for our more generalized system. Further, by linearizing the equations of motion, we characterize the entanglement present in the system, using the logarithmic negativity as a measure. We thereby characterize the changes in the system entanglement that result from the addition of a quadratic coupling to a linearly coupled system.

Contents

I. Introduction

Optomechanical systems focus on the interaction between light and matter [1, 2]. The typical optomechanical setup consists of an optical resonator that can confine one or more modes of electromagnetic radiation, and a mechanically pliant object which can be combined with that resonator. A simple example is an optical cavity made of two mirrors, one of which is fixed, while the other is mounted as a simple harmonic oscillator. Although simple in design, this system can exhibit rather rich behavior, including multistability, regenerative oscillations, photon blockade, cooling of mechanical motion, and storage of optical signals [1]. Typically, these phenomena can be observed when the optical cavity is excited by a strong driving laser [3].

This thesis investigates an optomechanical system with a focus on the stability conditions and entanglement, using a quintic equation. This quintic equation describes a system with a negative non-zero quadratic coupling. In Section II the physical model corresponding to this system and the resulting equations of motion are introduced. In Section III the steady-state analysis of the equations of motion are discussed. The model of the system is then provided when there is only linear coupling and a stability analysis is presented. A model of the system is then presented when both linear and quadratic coupling are present. The analysis of the steady state continues by deriving the solutions to the quintic by means of Tschirnhausen and canonical transformations, and hypergeometric equations. The resulting critical points are analyzed in terms of the input and output variables of the problems. The critical points are determined analytically as well as numerically. In Section IV, the fluctuations that occur within the system are analyzed by inspecting the covariance matrix, the dynamical stability, and the entanglement. The summary of these results and possible future investigations are provided in Section V.

II. Hamiltonian and Equations of Motion

The use of the Fabry-Perot cavity in optomechanics is well studied [4], where typically the cavity consists of two fixed mirrors that create a standing wave pattern. The focal lengths of the mirrors and the distance between them must be chosen appropriately in order for the beam inside the cavity to remain stable. This is known as a Fabry-Perot interferometer system, which consists of a pair of partially reflective glass facing each other, or a Fabry-Perot etalon system, which consists of a single plate with two parallel reflecting surfaces. However, the classic Fabry-Perot etalon system can be modified to include a movable semi-transmissive membrane that is suspended in the middle of the cavity, shown in Figure 1 [5, 6]. This membrane-in-the-middle cavity will be the one considered in this study, where the elements within the system are assumed to not absorb any of the light. The semi-transmissive membrane allows some light to pass through while reflecting the rest. The study of this Fabry-Perot cavity is carried out when both linear and quadratic coupling between light and mechanics are present [1]. The input intensity of the laser into the cavity interacts with the membrane and causes the resonant frequency of the cavity to change as the membrane moves. The quantum mechanical Hamiltonian of the relevant system has the form,

$$H = \hbar\Delta_\circ \hat{a}^\dagger \hat{a} + \frac{1}{2}\hbar\omega_m(\hat{p}^2 + \hat{q}^2) - \hbar G_L \hat{a}^\dagger \hat{a}\hat{q} + \hbar G_Q \hat{a}^\dagger \hat{a}\hat{q}^2 + i\hbar E(\hat{a}^\dagger - \hat{a}), \tag{II.1}$$

where the operators obey the canonical commutation relations $[\hat{a}, \hat{a}^\dagger] = 1$, and $[\hat{q}, \hat{p}] = i$

Note: In Eq. (1) each variable is named as follows,

$\hat{q}$ - Position Operator of the mechanical part,

$\hat{p}$ - Momentum Operator of the mechanical part,

$\hat{a}$ - Photon Annihilation Operator,

$\hat{a}^\dagger$ - Photon Creation Operator,

ω_m - Mechanical Frequency,

G_L - Linear Coupling Constant,

G_Q - Quadratic Coupling Constant,

$\Delta_\circ = \omega_c - \omega_L$ - Detuning between the incident radiation and optical cavity,

ω_c - Cavity Frequency,

ω_L - Laser Frequency,

E - Energy coupling of laser driving cavity

$\hbar$ - Planck's Constant.

In (II.1) the first term corresponds to the energy of the bare optical mode, the second term describes

the kinetic and potential energies of the mechanical oscillator, the third and fourth terms arise from the linear and quadratic couplings, respectively, of the mechanical oscillator amplitude to the optical field, and the fifth term is due to the external driving laser.

The system can be described by Figure 1 below,

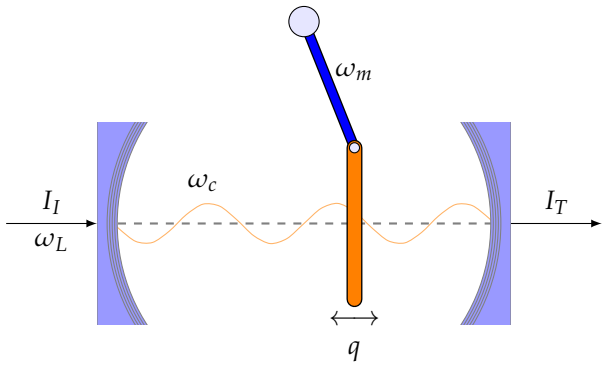

Figure 1: Fabry-Perot cavity with a movable membrane hung in the middle. The value of q is the distance that the membrane deviates from its equilibrium point, I_I is the input intensity of the laser, I_T is the intensity transmitted by the cavity, and ω_L is the laser frequency.

The time evolution of any dynamical variable $\hat{A}(t)$ can be found from the Heisenberg equation [7],

$$\frac{\mathrm{d}\hat{A}(t)}{dt} = \frac{i}{\hbar}\left[\hat{H}, \hat{A}(t)\right] + \frac{\partial \hat{A}(t)}{\partial t}.$$

The equations of motion of the dimensionless position, momentum and photon annihilation operators respectively are:

$$\dot{\hat{q}} = \omega_m \hat{p}, \tag{II.2}$$

$$\dot{\hat{p}} = -\omega_m \hat{q} + G_L \hat{a}^\dagger \hat{a} - 2G_Q \hat{a}^\dagger \hat{a} \hat{q} - \gamma_m \hat{p} + \xi(t), \tag{II.3}$$

$$\dot{\hat{a}} = -i\Delta_\circ \hat{a} + iG_L \hat{a}\hat{q} - iG_Q \hat{a}\hat{q}^2 + E - \kappa \hat{a} + \sqrt{2\kappa}\hat{a}_{in}, \tag{II.4}$$

where the damping and noise terms,

κ - Optical Decay Rate of the Cavity,

γ_m - Mechanical Damping Rate,

ξ - Thermal Langevin Noise Force,

$\xi(t)$ - Noise associated with the Damping of the Mechanical Oscillator, and

$\hat{a}_{in}$ - Vacuum Input Noise of the Cavity,

have been added following the prescription of Quantum Langevin theory [3, 8]. The correlation

functions for a_{in} and ξ respectively are as follows [9],

$$< a_{in}(t)a_{in}^{\dagger}(t) >= [\delta(t-t')],$$
$$< \xi(t)\xi(t') >= \frac{\gamma_m}{\omega_m}\int \frac{\omega}{2*\pi}e^{-i\omega(t-t')}\left[coth\left(\frac{\hbar\omega}{2k_BT}+1\right)\right]\mathrm{d}\omega.$$

In Eqs. (II.2)-(II.3), G_L and G_Q are defined as,

$$G_L = g_L\sqrt{\frac{\hbar}{m\omega_m}},$$
$$G_Q = \frac{g_Q\hbar}{m\omega_m}, \tag{II.5}$$

where m is the effective mass of the membrane.

III. Steady State

III.1 Derivation of Optomechanical Quintic Equation

We assume the existence of classical steady-state solutions which are found by setting (II.2), (II.3), and (II.4), respectively, equal to zero,

$$0 = \omega_m p_s, \tag{III.1}$$

$$0 = -\omega_m q_s + G_L a_s^* a_s - 2G_Q a_s^* a_s q_s - \gamma_m p_s, \tag{III.2}$$

$$0 = -i\Delta_\circ a_s + iG_L a_s q_s - iG_Q a_s q_s^2 + E - \kappa a_s, \tag{III.3}$$

where a_s, p_s, and q_s are the classical steady-state values of their respective variables. Solving (III.3) for a_s and then taking the modulus of the resulting equation provides,

$$|a_s|^2 = \frac{|E|^2}{\kappa^2 + [\Delta_\circ - G_L q_s + G_Q q_s^2]^2}. \tag{III.4}$$

From (III.1) solving for p_s yields,

$$p_s = 0. \tag{III.5}$$

We note that due to the momentum in the steady-state, p_s, being equal to zero, the mechanical damping, γ_m, does not affect the steady-state of the system. Substituting this value of p_s into (III.2) and solving for q_s results in,

$$q_s = \frac{G_L |a_s|^2}{\omega_m + 2G_Q |a_s|^2}. \tag{III.6}$$

We define the denominator of q_s as the effective mechanical frequency,

$$\omega_{eff} = \omega_m + 2G_Q |a_s|^2. \tag{III.7}$$

Substituting q_s into (III.4) formulates the general optomechanical equation,

$$|a_s|^2 = \frac{|E|^2}{\kappa^2 + \left[\Delta_\circ - G_L \left[\frac{G_L |a_s|^2}{\omega_m + 2G_Q |a_s|^2}\right] + G_Q \left[\frac{G_L |a_s|^2}{\omega_m + 2G_Q |a_s|^2}\right]^2\right]^2}. \tag{III.8}$$

Although this is the general form, in the following equations the variables within the optomechanical equation will be scaled by mechanical frequency (ω_m). By dividing (III.7) by ω_m^2 and with some manipulation, we obtain the following dimensionless formulation,

$$\left(\frac{\kappa}{\omega_m}\right)^2 |a_s|^2 + |a_s|^2 \left(\frac{\Delta_\circ}{\omega_m} - \frac{G_L}{\omega_m}\left[\frac{\frac{G_L}{\omega_m}|a_s|^2}{1 + 2\frac{G_Q}{\omega_m}|a_s|^2}\right] + \frac{G_Q}{\omega_m}\left[\frac{\frac{G_L}{\omega_m}|a_s|^2}{1 + 2\frac{G_Q}{\omega_m}|a_s|^2}\right]^2\right)^2 = \left(\frac{|E|}{\omega_m}\right)^2. \tag{III.9}$$

The form of the optomechanical equation being sought needs to be expressed in terms of the input intensity and the transmitted intensity, to obtain this form the substitutions of the following need to be made into equation (III.8),

$$I_I = \left(\frac{|E|}{\omega_m}\right)^2, \tag{III.10}$$

$$I_T = \frac{\kappa}{\omega_m}|a_s|^2. \tag{III.11}$$

With these substitutions, the dimensionless quintic equation is found to be,

$$\frac{\kappa}{\omega_m}I_T + \frac{\omega_m}{\kappa}I_T\left(\frac{\Delta_\circ}{\omega_m} - \frac{G_L}{\omega_m}\left[\frac{\frac{G_L}{\omega_m}\frac{\omega_m}{\kappa}I_T}{1+2\frac{G_Q}{\omega_m}\frac{\omega_m}{\kappa}I_T}\right] + \frac{G_Q}{\omega_m}\left[\frac{\frac{G_L}{\omega_m}\frac{\omega_m}{\kappa}I_T}{1+2\frac{G_Q}{\omega_m}\frac{\omega_m}{\kappa}I_T}\right]^2\right)^2 = I_I. \tag{III.12}$$

For reasons of simplicity, some further changes of variables are made to equation (III.11) resulting finally in,

$$AI_T + BI_T\left(C - D\left[\frac{H_1 I_T}{H_2 + H_3 I_T}\right] + E\left[\frac{H_1 I_T}{H_2 + H_3 I_T}\right]^2\right)^2 = I_I, \tag{III.13}$$

where,

$$A = \frac{\kappa}{\omega_m}, \quad B = \frac{\omega_m}{\kappa}, \quad C = \frac{\Delta_\circ}{\omega_m}, \quad D = \frac{G_L}{\omega_m},$$
$$E = \frac{G_Q}{\omega_m}, \quad H_1 = \frac{G_L}{\omega_m}\frac{\omega_m}{\kappa}, \quad H_2 = 1, \quad H_3 = 2\frac{G_Q}{\omega_m}\frac{\omega_m}{\kappa}. \tag{III.14}$$

III.2 Linear Coupling Only

When the scaled quadratic coupling (G_Q/ω_m) is equal to zero, the quintic from equation (III.12) reduces to a cubic [4]. Using values found from [3], the graph of the cubic is created and the hysteresis loop of the intracavity intensity is shown in Figure 2.

It can be seen from Figure 2 that for a single value of I_I multiple values of I_T exist within the region of bistability. This is the phenomenon of multistability. However, not all resulting values of I_T are stable solutions. The definition of stability will be provided, and the steps required to demonstrate stability will be carried out, in Section III.4. Using the steps in Section III.4 for determining stability, and applying the linear coupling constraints the results achieved in [3] pertaining to the cubic were duplicated. Specifically, the cubic is stable on branch S_1, which extends from the origin to the first stationary point (denoted by CSP_1); and on branch S_3, which extends from the second stationary point (denoted by CSP_2) to infinity. The center branch denoted by S_2 is unstable and extends between the two stationary points CSP_1 and CSP_2.

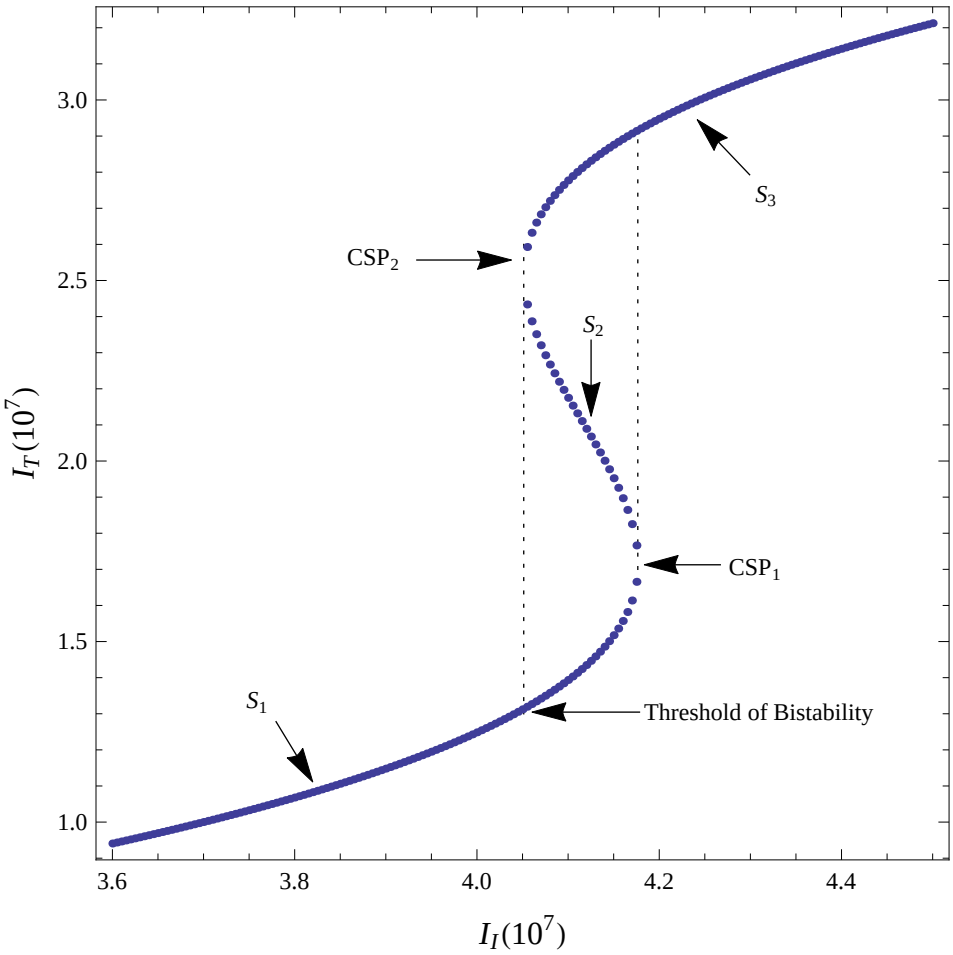

Figure 2: Optomechanical Bistable Cubic, where I_I and I_T are dimensionless quantities. The parameters used are, $\kappa/\omega_m = 1.4$, $G_L/\omega_m = 3.4 * 10^{-4}$, $G_Q/\omega_m = 0$, $\Delta_\circ/\omega_m = 2.62$, and $\omega_m = 10^7 Hz$ [1]. The region of bistability lies between the vertical dotted lines. The notations CSP_1 and CSP_2 indicate the stable saddle node bifurcations and S_1, S_2, and S_3 are the branches.

III.3 Linear and Quadratic Coupling

We now move from the case where $G_Q = 0$, to investigate the case where the quadratic coupling does not equal zero ($G_Q/\omega_m \neq 0$), as it corresponds to experiments where it cannot be ignored [10]. Using the values from [3] and $G_Q/\omega m < 0$, a typical graph of the optomechanical quintic is shown in Figure 3.

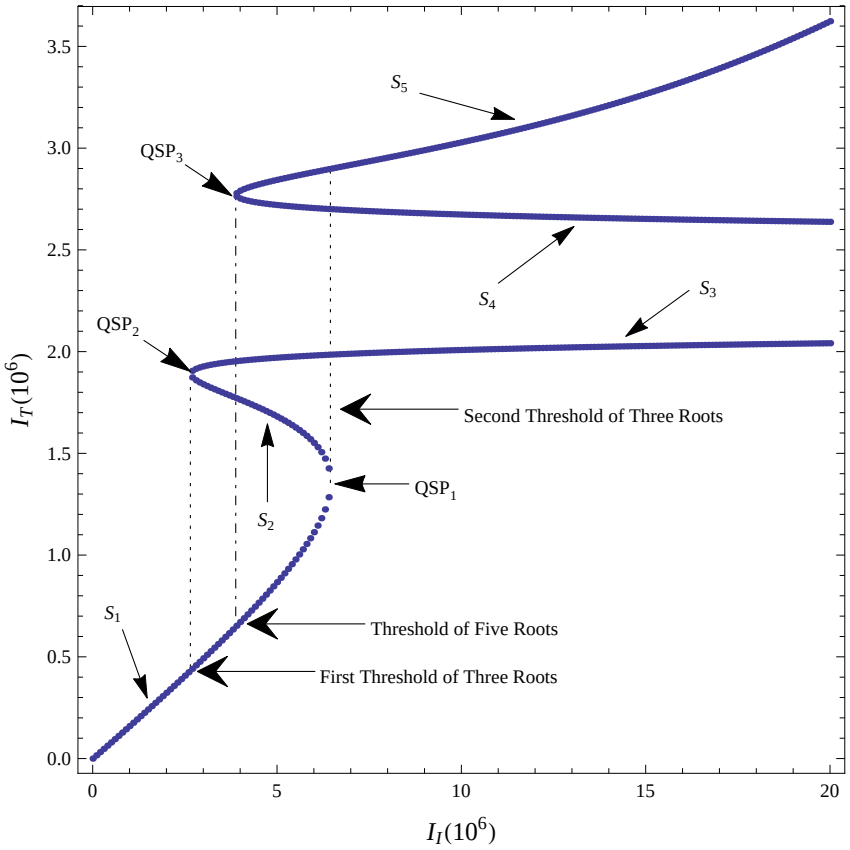

Figure 3: A plot of the Optomechanical Quintic (III.13), where I_I and I_T are dimensionless quantities. The parameters used are, $\kappa/\omega_m = 1.4$, $G_L/\omega_m = 3.4 * 10^{-4}$, $G_Q/\omega_m = -3 * 10^{-7}$, $\Delta_\circ/\omega_m = 2.62$, and $\omega_m = 10^7 Hz$. The labels QSP_1, QSP_2, and QSP_3 denote the stationary points of the quintic. The branches are defined as S_1 (which runs from 0 to QSP_1), S_2, S_3, S_4, and S_5 respectively.

As shown, when a small negative quadratic coupling ($G_Q/\omega_m < 0$) is added into the system, (III.11) forms a quintic resulting in Figure 3 above. The quintic is stable on branch S_1, which extends from the origin to QSP_1. The quintic is unstable on all of the remaining branches: S_2, which extends from QSP_1 to QSP_2; S_3, extending from QSP_2 to essentially infinity; S_4, which extends from infinity to QSP_3; and on branch S_5, extending from QSP_3 to infinity [4]. In comparing the quintic ($G_Q/\omega_m \neq 0$) in Figure 3 to that of the cubic ($G_Q/\omega_m = 0$) in Figure 2, it can be seen that both display regions where multiple values of I_T occur for a single value of I_I. However, we find the resulting stability of the equations differ greatly. The cubic, within the region where multiple values of I_T occur, has two stable branches and a single unstable branch. The quintic, within the region where multiple values of I_T occur, results in a single stable branch with all

remaining branches within the region being unstable. Similar curves as Figure 3 have been seen in other systems [11, 12].

When a positive quadratic coupling ($G_Q/\omega_m > 0$) is added to the system, there are no detectable regimes where more than one root occurs for values of G_Q/ω_m larger than 10^{-8} as shown in Figure 4.

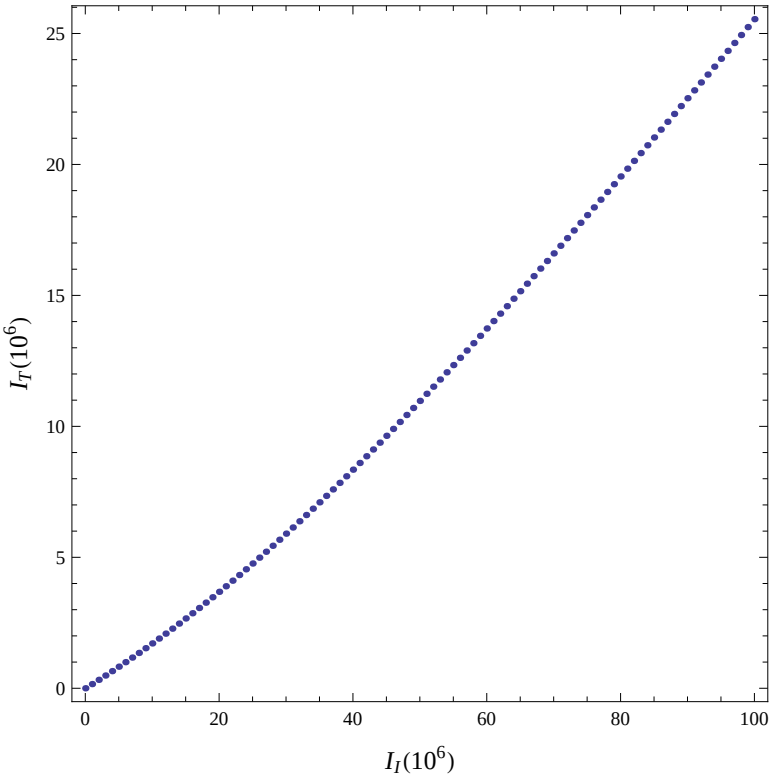

Figure 4: A plot of the Optomechanical Quintic (III.13), where I_I and I_T are dimensionless quantities. The parameters used are, $\kappa/\omega_m = 1.4$, $G_L/\omega_m = 3.4 * 10^{-4}$, $G_Q/\omega_m = 3 * 10^{-8}$, $\Delta_\circ/\omega_m = 2.62$, and $\omega_m = 10^7 Hz$.

III.4 Stability Analysis

The stability of the branches in Figure 3 was established by inspecting the eigenvalues of the Jacobian matrix for a point (I_I, I_T) on each branch [13]. To find the Jacobian and resulting eigenvalues, equations (III.10) and (III.11) are solved to find the values of E and $|a_s|^2$ as described below. These values are then substituted into (III.6) to solve for q_s which in turn is substituted into (III.3) to find a_s which is separated into it's real (x_s) and complex (y_s) parts. The steady-state

values are substituted into the Jacobian matrix (J), which is formulated from (II.2) - (II.4), and the resulting eigenvalues are determined.

In order to formulate the Jacobian matrix in the manner of classical dynamical systems [13], equation (II.4) is split into its real and complex parts creating new equations in $\dot{x}$ and $\dot{y}$, i.e. $\dot{a} = \dot{x} + i\dot{y}$. Thus, equations (II.2) - (II.4) are written as,

$$\dot{q} = \omega_m p, \tag{III.15}$$

$$\dot{p} = -\omega_m q + G_L(x^2 + y^2) - 2G_Q(x^2 + y^2)q - \gamma_m p, \tag{III.16}$$

$$\dot{x} = \Delta_\circ y - G_L y q + G_Q y q^2 + E - \kappa x, \tag{III.17}$$

$$\dot{y} = -\Delta_\circ x + G_L x q - G_Q x q^2 - \kappa y. \tag{III.18}$$

In order to form the Jacobian, which generalizes the gradient, the partial derivative of each equation of motion (III.15) - (III.18) is taken with respect to the dynamical variables of the problem. The general form of the Jacobian is,

$$J = \begin{bmatrix} \frac{\partial \dot{q}}{\partial q} & \frac{\partial \dot{q}}{\partial p} & \frac{\partial \dot{q}}{\partial x} & \frac{\partial \dot{q}}{\partial y} \\ \frac{\partial \dot{p}}{\partial q} & \frac{\partial \dot{p}}{\partial p} & \frac{\partial \dot{p}}{\partial x} & \frac{\partial \dot{p}}{\partial y} \\ \frac{\partial \dot{x}}{\partial q} & \frac{\partial \dot{x}}{\partial p} & \frac{\partial \dot{x}}{\partial x} & \frac{\partial \dot{x}}{\partial y} \\ \frac{\partial \dot{y}}{\partial q} & \frac{\partial \dot{y}}{\partial p} & \frac{\partial \dot{y}}{\partial x} & \frac{\partial \dot{y}}{\partial y} \end{bmatrix}. \tag{III.19}$$

The Jacobian matrix evaluates to,

$$J = \begin{bmatrix} 0 & \omega_m & 0 & 0 \\ -\omega_m - 2G_Q(x^2 + y^2) & -\gamma_m & 2G_L x - 4G_Q q x & 2G_L y - 4G_Q q y \\ -G_L y + 2G_Q q y & 0 & -\kappa & -G_L q + G_Q q^2 + \Delta_0 \\ -G_L x + 2G_Q q x & 0 & G_L q - G_Q q^2 - \Delta_0 & -\kappa \end{bmatrix}. \tag{III.20}$$

It is of interest to note that the first and second stationary points (QSP_1, and QSP_2) are stable and the third stationary point (QSP_3) is unstable. The stability of each node in Figure 3 is determined by finding the eigenvalues of the Jacobian matrix where a negative eigenvalue results in a stable point and a positive results in an unstable point. This results in the stationary points being classifiable. We find that QSP_1 is as a stationary stable saddle node, QSP_2 is a stationary stable node, and QSP_3 is a stationary unstable node.

III.5 Analytic Solution to Quintic

It is possible to find the roots of the quintic equation (III.12) analytically using special functions [14, 15, 16]. However, to do so, Tschirnhausen transformations must be implemented. The following

steps outline the process for solving the quintic analytically:

1: The resultant of the quadratic Tschirnhausen transformation and the general quintic is taken to form a new quintic in y.
2: The principal quintic in y is formed.
3: Once the principal quintic is formed, the resultant of the principal quintic and the quartic Tschirnhausen is taken to form a new quintic in terms of z.
5: After simplifying, the Bring-Jerrard quintic in z is formed.
6: Now that the Bring-Jerrard is formed, the Bring-Jerrard normal form can be formed using the canonical transform. This is a linear transformation that sets the constant coefficient of the second order term equal to 1.
7: This allows hypergeometric functions to be used, allowing the Bring-Jerrard normal form to be solved.
8: Once the solutions are found, the Tschirnhausen transformations need to be inverted to solve the original quintic.

The reader is referred to Appendix A for a more complete description of the process outlined above.

III.6 Critical Points: Dependence on I_I

The behavior of the system with respect to I_I is of interest, as I_I is an input variable. In order to examine this behavior, we will consider (III.13) with I_I as an independent variable. The paper titled On The Number of Real Roots of a Quintic Equation [17] outlines the requirements for the quintic equation to have 1, 3 or 5 real roots. All of these regimes can be seen in Figure 3. To determine the number of real roots, which will be referred to as 'stationary points' in the case of the quintic, the general quintic, (III.13), must be transformed in such a way as to drop the fourth order term. The general quintic and the corresponding transformation are shown below.

$$a_0x^5 + 5a_1x^4 + 10a_2x^3 + 10a_3x^2 + 5a_4x + a_5 = 0, \tag{III.21}$$

$$x \to \frac{T - a_1}{a_0}, \tag{III.22}$$

where the parameters a_0, a_1, a_2, a_3, a_4, and a_5 are in terms of A, B, C, D, E, $H1$, $H2$, and $H3$. This transformation creates a new quintic in T,

$$T^5 + 10A_2 + T^3 + 10A_3T^2 + 5A_4T + A_5 = 0, \tag{III.23}$$

where A_2, A_3, A_4, and A_5 are in terms of a_0, a_1, a_2, a_3, a_4, and a_5. Equation (III.23) can be written in the form,

$$T^5 + 10A_2 + T^3 + 10A_3T^2 + 5\mathcal{Y}T + \mathcal{X} = 0, \tag{III.24}$$

and then be interpreted as a straight line, depending on the variable parameter T, in the Cartesian $(\mathcal{X}, \mathcal{Y})$ plane. The variables $\mathcal{X}$ and $\mathcal{Y}$ are defined as follows,

$$\begin{aligned} \mathcal{X} =& 4T^5 + 20A_2T^3 + 10A_3T^2, \\ \mathcal{Y} =& -T^4 - 6A_2T^2 - 4A_3T. \end{aligned} \tag{III.25}$$

The criteria outlined by Chaundy [17] are shown in Table 5 (in our case roots refer to the stationary points),

Five Real Roots:	$\Delta \geq 0$,	$4A_2^3 + A_3^2 \leq 0$,	$\Theta \leq 0$;
	$\Delta = 0$,	$4A_2^3 + A_3^2 = 0$,	$\Theta = 0$;
Three Real and Two Imaginary Roots:	$\Delta < 0$;		
	$\Delta = 0$,	$4A_2^3 + A_3^2 > 0$;	
		$4A_2^3 + A_3^2 = 0$,	$\Theta \neq 0$;
		$4A_2^3 + A_3^2 < 0$,	$\Theta > 0$;
One Real and Four Imaginary Roots:	$\Delta > 0$,	$4A_2^3 + A_3^2 \geq 0$;	
		$4A_2^3 + A_3^2 < 0$,	$\Theta > 0$;

Table 1: Analytic Conditions to determine one, three, or five real roots of equation (III.23). Column wise, the first condition is of the discriminant, the second condition is a coefficient constraint and the third condition is of the conic equation [17].

The discriminant, Δ, can be formed from (III.23). The second condition, shown in Table 1, defines a restriction using coefficients A_2 and A_3 from (III.23). The quantity Θ, is known as the *conic* and is given by,

$$\Theta = -y\left(272A_2^3 - 108A_3^2\right) + 24A_2^2\left(40A_2^3 + 27A_3^2\right) - 76A_2A_3x + 16A_2y^2 + x^2. \tag{III.26}$$

In principal, the criterion in Table 1 can be used to analytically determine the number of roots in each region of our problem. However, they are not always convenient to use.

III.7 Critical Points: Dependence on I_T

III.7.1 Analytical Treatment

The analysis of the system behavior with respect to I_T is of interest, as I_T is an output variable. In order to examine this behavior, we will consider (III.12) with I_T as an independent variable. As is specific to equations of optomechanical systems that result in multistable regimes, the graphical plots of these equations have critical points, i.e. points where the derivative of I_I with respect to I_T (dI_I/dI_T) is equal to zero or is undefined, that occur on the y-axis [4]. This can be seen at the points QSP_1, QSP_2, and QSP_3 in Figure 3. The quintic equation is no exception, and the critical points define the thresholds of the quintic. The unique aspect of the quintic, however, is that one of the critical points that occurs is observed to appear essentially at infinite input intensity (I_I). This is similar to results in [18] where a single saddle node bifurcation is located near the end of their domain.

The following will go through the steps in determining the locations of these critical points. Starting with the optomechanical quintic equation (III.12), the derivative with respect to I_T is taken, resulting in the following equation,

$$A + BC^2 + \frac{2BCDH_1H_3I_T^2}{(H_2+H_3I_T)^2} - \frac{4BCDH_1I_T}{H_2+H_3I_T} - \frac{4BCEH_1^2H_3I_T^3}{(H_2+H_3I_T)^3} + \frac{6BCEH_1^2I_T^2}{(H_2+H_3I_T)^2} - \frac{2BD^2H_1^2H_3I_T^3}{(H_2+H_3I_T)^3}$$
$$+\frac{3BD^2H_1^2I_T^2}{(H_2+H_3I_T)^2} + \frac{6BDEH_1^3H_3I_T^4}{(H_2+H_3I_T)^4} - \frac{8BDEH_1^3I_T^3}{(H_2+H_3I_T))^3} - \frac{4BE^2H_1^4H_3I_T^5}{(H_2+H_3I_T)^5} + \frac{5BE^2H_1^4I_T^4}{(H_2+H_3I_T)^4} = \frac{dI_I}{dI_T}.$$

(III.27)

Setting the derivative equal to zero in order to find the critical points with respect to the variable I_T results in,

$$A + BC^2 + \frac{2BCDH_1H_3I_T^2}{(H_2+H_3I_T)^2} - \frac{4BCDH_1I_T}{H_2+H_3I_T} - \frac{4BCEH_1^2H_3I_T^3}{(H_2+H_3I_T)^3} + \frac{6BCEH_1^2I_T^2}{(H_2+H_3I_T)^2} - \frac{2BD^2H_1^2H_3I_T^3}{(H_2+H_3I_T)^3}$$
$$+\frac{3BD^2H_1^2I_T^2}{(H_2+H_3I_T)^2} + \frac{6BDEH_1^3H_3I_T^4}{(H_2+H_3I_T)^4} - \frac{8BDEH_1^3I_T^3}{(H_2+H_3I_T))^3} - \frac{4BE^2H_1^4H_3I_T^5}{(H_2+H_3I_T)^5} + \frac{5BE^2H_1^4I_T^4}{(H_2+H_3I_T)^4} = 0.$$

(III.28)

This expression can be written as,

$$\frac{f}{g} = 0.$$

The numerator (f) can be written as,

$$\begin{aligned} f =& I_T^5\left(AH_3^5 + BC^2H_3^5 - 2BCDH_1H_3^4 + 2BCEH_1^2H_3^3 + BD^2H_1^2H_3^3 - 2BDEH_1^3H_3^2 + BE^2H_1^4H_3\right) \\ &+ I_T^4\left(5AH_2H_3^4 + 5BC^2H_2H_3^4 - 10BCDH_1H_2H_3^3 + 10BCEH_1^2H_2H_3^2 + 5BD^2H_1^2H_2H_3^2\right. \\ &\left. - 10BDEH_1^3H_2H_3 + 5BE^2H_1^4H_2\right) + I_T^3\left(10AH_2^2H_3^3 + 10BC^2H_2^2H_3^3 - 18BCDH_1H_2^2H_3^2\right. \\ &\left. + 14BCEH_1^2H_2^2H_3 + 7BD^2H_1^2H_2^2H_3 - 8BDEH_2^3H_2^2\right) + I_T^2\left(10AH_2^3H_3^2 + 10BC^2H_2^3H_3^2\right. \\ &\left. - 14BCDH_1H_2^3H_3 + 6BCEH_1^2H_2^3 + 3BD^2H_1^2H_2^3\right) + I_T\left(5AH_2^4H_3 + 5BC^2H_2^4H_3\right. \\ &\left. - 4BCDH_1H_2^4\right) + AH_2^5 + BC^2H_2^5, \end{aligned} \tag{III.29}$$

and the denominator (g) is shown below,

$$g = (H_2 + H_3I_T)^5. \tag{III.30}$$

Inspecting the function $g = 0$, allows the location of the complex critical turning point to be obtained. One finds $g = 0$ when $(H_2 + H_3I_T)^5 = 0$. This occurs at the critical transmitted intensity,

$$I_{T,c} = -\frac{H_2}{H_3}. \tag{III.31}$$

Using the relationships in (III.12), $I_{T,c}$ becomes, simply,

$$I_{T,c} = -\frac{\kappa}{2G_Q}. \tag{III.32}$$

We note that (III.31) is equivalent to the effective mechanical frequency (III.7) going to zero ($\omega_{eff} = 0$) for some critical value of $|a_{s,c}|^2$ as shown in the steps displayed below,

$$\begin{aligned} I_{T,c} &= -\frac{\kappa}{2G_Q}, \\ 2G_QI_{T,c} &= -\kappa, \end{aligned}$$

substituting in (III.11) and simplifying,

$$\begin{aligned} 2G_Q\frac{\kappa|a_{s,c}|^2}{\omega_m} &= -\kappa, \\ 2G_Q|a_{s,c}|^2 &= -\omega_m, \\ \omega_m + 2G_Q|a_{s,c}|^2 &= \omega_{eff} = 0. \end{aligned}$$

This value of $I_{T,c}$ will cause a division by zero in (III.28) resulting in a critical point. Substituting in the values that have been used throughout the paper into (III.31), $\kappa = 1.4\omega_m$ and $G_Q = -3 * 10^{-7}\omega_m$, $I_T = 2.33333 * 10^6$. The following plot of g, Figure 4, shows that when I_T is greater than $2.33333 * 10^6$, $g < 0$, and when I_T is less, $g > 0$.

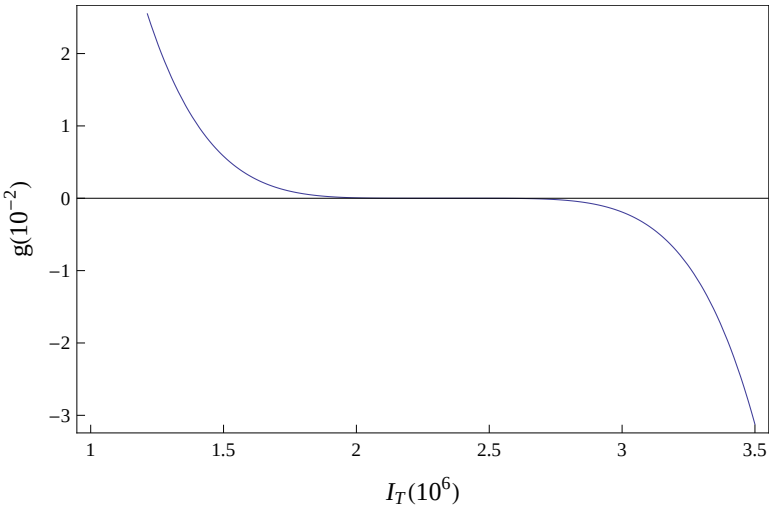

Figure 5: Characterization of the denominator function g as in (III.30), where I_T and g are dimensionless quantities. The parameters used are, $\kappa/\omega_m = 1.4$, $G_L/\omega_m = 3.4 * 10^{-4}$, $G_Q/\omega_m = 0$, $\Delta_\circ/\omega_m = 2.62$, and $\omega_m = 10^7 Hz$.

The analysis of the numerator function f will now be carried out to determine the characteristics of f, for which $f = 0$, $f < 0$, and $f > 0$. This will demonstrate generally how (III.28) behaves and specifically where the stationary turning points are. This is done numerically. First, solving for $f = 0$ we find the results stated in Table 2,

$I_T \to 1.35797 * 10^6$
$I_T \to 1.89040 * 10^6$
$I_T \to 2.77049 * 10^6$
$I_T \to 2.82390 * 10^6 - 1.10231 * 10^6 i$
$I_T \to 2.82390 * 10^6 + 1.10231 * 10^6$i

Table 2: Stationary Points of f (III.29), where I_T is a dimensionless quantity. The parameters used are, $\kappa/\omega_m = 1.4$, $G_L/\omega_m = 3.4 * 10^{-4}$, $G_Q/\omega_m = -3 * 10^{-7}$, $\Delta_\circ/\omega_m = 2.62$, and $\omega_m = 10^7 Hz$.

The results for $f > 0$ and $f < 0$ respectively are shown in Table 3.

$f > 0$	$0 \leq I_T < 1.35797 * 10^6$ or $1.89040 * 10^6 < I_T < 2.77049 * 10^6$
$f < 0$	$1.35797 * 10^6 < I_T < 1.89040 * 10^6$ or $I_T > 2.77049 * 10^6$

Table 3: Positive and Negative Ranges of f as in (III.29), where I_T is dimensionless quantities. The parameters used are, $\kappa/\omega_m = 1.4$, $G_L/\omega_m = 3.4 * 10^{-4}$, $G_Q/\omega_m = -3 * 10^{-7}$, $\Delta_\circ/\omega_m = 2.62$, and $\omega_m = 10^7 Hz$.

Now that f has been characterized, a graph showing the behavior of the numerator can be displayed, as in Figure 6.

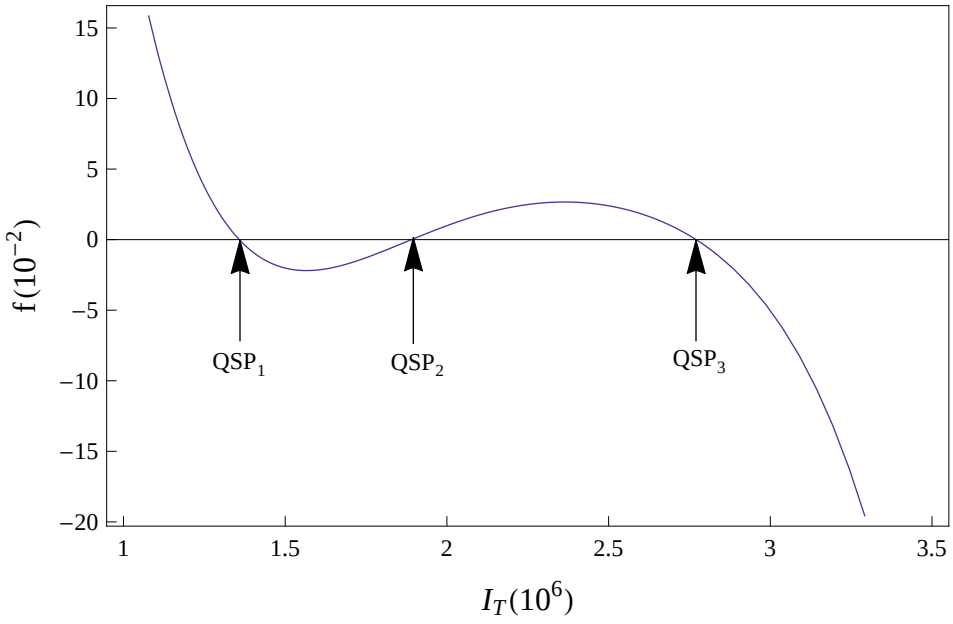

Figure 6: Characterization of the numerator function f (III.29), where I_T and f are dimensionless quantities. The parameters used are, $\kappa/\omega_m = 1.4$, $G_L/\omega_m = 3.4 * 10^{-4}$, $G_Q/\omega_m = 0$, $\Delta_\circ/\omega_m = 2.62$, and $\omega_m = 10^7 Hz$. The QSP refer to Figure 3.

These roots of the derivative function correlate to the stationary points of the optomechanical quintic, which are found numerically in Section III.7.2. Plotting the derivative function (f/g) in Figure 7 shows the behavior of the function, including its complex critical point, over the range of supportable values of I_T.

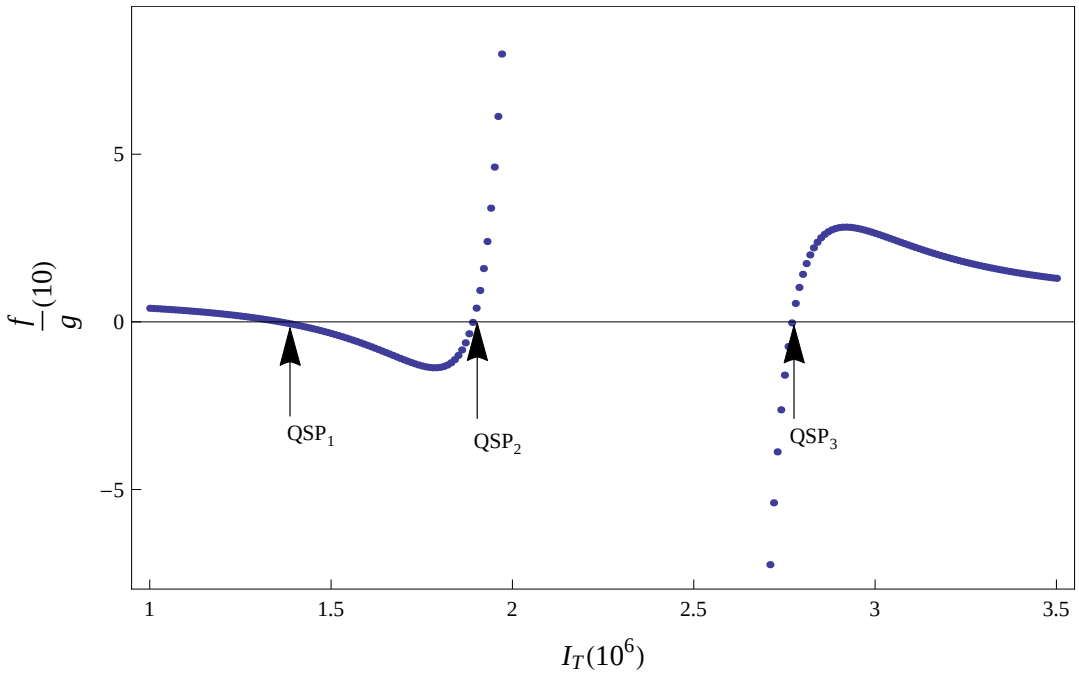

Figure 7: Characterization of the derivative function (III.27), where I_T and f/g are dimensionless quantities. The parameters used are, $\kappa/\omega_m = 1.4$, $G_L/\omega_m = 3.4 * 10^{-4}$, $G_Q/\omega_m = 0$, $\Delta_\circ/\omega_m = 2.62$, and $\omega_m = 10^7 Hz$. The QSP refer to Figure 3.

III.7.2 Numerical Solution

Using the derivative from (III.28), the locations of the critical points will now be determined. Due to the derivative being another fifth order equation, in principle the analytic solutions can be found by using the Tschirnhausen transformations and resulting hypergeometric solutions. For purposes of convenience, the derivative is solved numerically, using values found in [3] again with the addition of a small quadratic coupling, $G_Q/\omega_m = -3 * 10^{-7}$ to create the quintic equation. The resulting critical point list (CPL) in Table 4, shows all of the solutions to (III.13) where the first element is the location of the input intensity (I_I) and the second element is the transmitted intensity (I_T). The list orders the location of the critical and stationary points in the order in which they occur,

$I_I(10^6)$	$I_T(10^6)$
2.64906	1.8904
3.88025	2.77049
6.44776	1.35797
$2.02053 - 1.15672i$	$2.8239 - 1.10231i$
$2.02053 + 1.15672i$	$2.8239 + 1.10231i$

Table 4: Critical Point List (CPL), where I_I and I_T are dimensionless quantities. The parameters used are, $\kappa/\omega_m = 1.4$, $G_L/\omega_m = 3.4 * 10^{-4}$, $G_Q/\omega_m = -3 * 10^(-7)$, $\Delta_\circ/\omega_m = 2.62$, and $\omega_m = 10^7 Hz$.

These values of I_T in Table 4 correlate directly with those found in Table 2.

IV. Fluctuations

IV.1 Covariance Matrix

We now consider small fluctuations around the steady-state values in order to investigate the effect of small changes made to the system. The covariance matrix can be formed from the equations shown in (IV.2) and (IV.4). In order to extract the fluctuations, each dynamical variable is considered as the sum of a large classical steady-state and a small quantum fluctuation about that mean [19, 20]. Thus, we obtain

$$\begin{aligned} \hat{q} &= q_s + \delta\hat{q}, \\ \hat{p} &= p_s + \delta\hat{p}, \\ \hat{a} &= a_s + \delta\hat{a}. \end{aligned} \tag{IV.1}$$

These are substituted into the equations (II.2) - (II.4) and then the terms that are bilinear or higher in the fluctuations are dropped. This results in (IV.2),

$$\begin{aligned} \delta\dot{\hat{q}} =& \omega_m \delta\hat{p}, \\ \delta\dot{\hat{p}} =& -\left(\omega_m + 2G_Q|a_s|^2 - \frac{G^2\Delta}{(\kappa^2+\Delta^2)}\right)\delta\hat{q} - \gamma_m\delta\hat{p} + \delta\xi(t), \\ \delta\dot{\hat{a}} =& \frac{iG}{\sqrt{2}(\kappa+i\Delta)}\delta\hat{q}, \end{aligned} \tag{IV.2}$$

where G and Δ are defined as follows,

$$\begin{aligned} G =& \sqrt{2}(G_L a_s - 2G_Q q_s a_s), \\ \Delta =& \Delta_\circ - G_L q_s + G_Q q_s^2. \end{aligned} \tag{IV.3}$$

The $\delta\hat{x}$ and $\delta\hat{y}$ equations can be found, from the steady-state equations (III.1) - (III.3),

$$\begin{aligned} \delta\dot{\hat{x}} =& -\frac{\kappa}{\sqrt{2}}(\delta\hat{a} + \delta\hat{a}^\dagger) + (\Delta_\circ - G_L q_s + G_Q q_s^2)\frac{-i(\delta\hat{a} + \delta\hat{a}^\dagger)}{\sqrt{2}} + \sqrt{2\kappa}\frac{\delta\hat{a}_{in} + \delta\hat{a}_{in}^\dagger}{\sqrt{2}}, \\ \delta\dot{\hat{y}} =& -(\Delta_\circ - G_L q_s + G_Q q_s^2)\frac{\delta\hat{a} + \delta\hat{a}^\dagger}{\sqrt{2}} - \kappa\frac{i(\delta\hat{a} + \delta\hat{a}^\dagger)}{\sqrt{2}} + \frac{2(G_L a_s + 2G_Q a_s q_s)}{\sqrt{2}}\delta\hat{q} - \frac{i\sqrt{2\kappa}(\delta\hat{a}_{in} + \delta\hat{a}_{in}^\dagger)}{\sqrt{2}}. \end{aligned} \tag{IV.4}$$

The variables $\delta\hat{x}$ and $\delta\hat{y}$ are linear combinations of the photon annihilation, $\delta\hat{a}$, and photon creation, $\delta\hat{a}^\dagger$, operators and have the form,

$$\begin{aligned}
\delta\hat{x} =& \frac{\delta\hat{a} + \delta\hat{a}^\dagger}{\sqrt{2}}, \\
\delta\hat{y} =& \frac{-i(\delta\hat{a} - \delta\hat{a}^\dagger)}{\sqrt{2}}, \\
\delta\dot{\hat{x}} =& \frac{\delta\dot{\hat{a}} + \delta\dot{\hat{a}}^\dagger}{\sqrt{2}}, \\
\delta\dot{\hat{y}} =& \frac{-i(\delta\dot{\hat{a}} - \delta\dot{\hat{a}}^\dagger)}{\sqrt{2}}, \\
\delta\hat{x}_{in} =& \frac{\sqrt{2\kappa}(\delta\hat{a}_{in} + \delta\hat{a}_{in}^\dagger)}{\sqrt{2}}, \\
\delta\hat{y}_{in} =& \frac{-i\sqrt{2\kappa}(\delta\hat{a}_{in} - \delta\hat{a}_{in}^\dagger)}{\sqrt{2}}.
\end{aligned} \tag{IV.5}$$

The variables $\delta\hat{x}_{in}$ and $\delta\hat{y}_{in}$ can be expressed as combinations of $\delta\hat{a}_{in}$, $\delta\hat{a}_{in}^\dagger$. The equations in (V.2) and (V.4) can be written as,

$$\dot{U} = \begin{bmatrix} \delta\dot{\hat{q}} \\ \delta\dot{\hat{p}} \\ \delta\dot{\hat{x}} \\ \delta\dot{\hat{y}} \end{bmatrix} = A \begin{bmatrix} \delta\hat{q} \\ \delta\hat{p} \\ \delta\hat{x} \\ \delta\hat{y} \end{bmatrix} + \begin{bmatrix} 0 \\ \delta\xi \\ \delta\hat{x}_{in} \\ \delta\hat{y}_{in} \end{bmatrix}, \tag{IV.6}$$

where the coefficient matrix, A, is given by,

$$A = \begin{bmatrix} 0 & \omega_m & 0 & 0 \\ -2G_Q\,|a_s|^2 - \omega_m & -\gamma_m & G & 0 \\ 0 & 0 & -\kappa & \Delta \\ G & 0 & -\Delta & -\kappa \end{bmatrix}. \tag{IV.7}$$

It should be noted that the coefficient matrix A, (IV.7), is different from the Jacobian matrix, (III.20). The coefficient matrix is formed from a linearization of equations (II.2) - (II.4) while the Jacobian matrix is a generalization of the gradient on the equations of motion (III.15) - (III.18), and contains contributions non-linear in the dynamical variables. The covariance matrix, V, obeys the equation [3, 21, 22, 23, 24],

$$\dot{V} = AV + VA^T + D, \tag{IV.8}$$

where the dot in $\dot{V}$ signifies a derivative with respect to time. The matrix D is related to the noise correlation matrix and is found to be:

$$D = \begin{bmatrix} 0 & 0 & 0 & 0 \\ 0 & \left(1 + \frac{2}{e^{(\hbar\omega_m/k_BT)}-1}\right)\gamma_m & 0 & 0 \\ 0 & 0 & \kappa & 0 \\ 0 & 0 & 0 & \kappa \end{bmatrix}, \tag{IV.9}$$

where T is the ambient temperature and k_B is Boltzmann constant. Since the steady-state is of interest, we set $\dot{V} = 0$ and this allows the elements with the matrix V to be solved for,

$$0 = AV + VA^T + D. \tag{IV.10}$$

We find V has the form [22],

$$V = \begin{bmatrix} \Lambda 1 & s & l & v \\ s & \Lambda 2 & o & r \\ l & o & \Lambda 3 & d \\ v & r & d & \Lambda 4 \end{bmatrix}. \tag{IV.11}$$

The matrix elements are cumbersome in form and will not be presented here.

IV.2 Dynamical Stability

Stability refers to a time-independent state of motion while dynamic stability refers to a time-dependent state of motion. This dynamic stability is quantified by the Routh-Hurwitz criterion [25]. This criterion provides a way to determine if the equations of motion in a system have only stable solutions. In order for the present system to be stable, the Routh-Hurwitz criterion implies the following inequalities,

$$\gamma_m + 2\kappa > 0, \tag{IV.12}$$

$$2\gamma_m G_Q |a|^2 \omega_m + 2\kappa\left(\gamma_m^2 + 2\gamma_m\kappa + \Delta^2 + \kappa^2\right) + \gamma_m\omega_m^2 > 0, \tag{IV.13}$$

$$\begin{aligned} &\omega_m\left(8\gamma_m G_Q\kappa |a|^2\left(\kappa(\gamma_m+\kappa) - \Delta^2\right) + \Delta G^2(\gamma_m+2\kappa)^2\right) \\ &\quad + 4\gamma_m\kappa\omega_m^2\left(2G_Q^2|a|^4 + \kappa(\gamma_m+\kappa) - \Delta^2\right) + 8\gamma_m G_Q\kappa|a|^2\omega_m^3 \\ &\quad + 2\gamma_m\kappa\left(\Delta^2+\kappa^2\right)\left(\gamma_m^2 + 2\gamma_m\kappa + \Delta^2 + \kappa^2\right) + 2\gamma_m\kappa\omega_m^4 > 0, \end{aligned} \tag{IV.14}$$

$$\omega_m\left(\left(\Delta^2+\kappa^2\right)\omega_m + 2G_Q|a|^2\left(\Delta^2+\kappa^2\right) - \Delta G^2\right) > 0. \tag{IV.15}$$

IV.3 Entanglement

Now that the covariance matrix has been found and the Routh-Hurwitz stability criteria have been formulated, the optomechanical entanglement can be quantified. Quantum Entanglement corresponds to the presence of nonclassical correlations between two objects. It is of interest as it is a resource for quantum computation. It is also of interest intrinsically as a not-yet-well-understood aspect of quantum mechanics. Its observation at the macroscopic scale is a current experimental aim and optomechanical systems seem to be a promising platform for such observations. Thus, it is of importance to characterize the entanglement in our system. Within our system continuous variable entanglement exists, and requires taking into account the dissipative nature of the system. The characteristics of the entanglement between the mechanics and the light field, can be found once the correlations between the mechanical and optical quadratures are known [1]. These correlations between the mechanical motion and the light beam are described by the covariance matrix (IV.11). To solve for the entanglement, the covariance matrix formulated above by (IV.11) is first written as,

$$V = \begin{bmatrix} \mathcal{A} & \mathcal{C} \\ \mathcal{C}^{\mathsf{T}} & \mathcal{B} \end{bmatrix}. \tag{IV.16}$$

The smallest symplectic eigenvalue (ν_{min}) of this matrix, satisfies the condition of,

$$V^T \Omega V = \Omega, \tag{IV.17}$$

where,

$$\Omega = \begin{bmatrix} 0 & I_n \\ -I_n & 0 \end{bmatrix}, \tag{IV.18}$$

and I_n is the n x n identity matrix ($n = 4$, in the present case). The smallest symplectic eigenvalue of the partially transposed covariance matrix V, can then be defined as [3],

$$\nu_{min} = \left[\frac{1}{2}(\Sigma - \sqrt{\Sigma^2 - 4 \det V})\right]^{\frac{1}{2}}, \tag{IV.19}$$

where $\Sigma = \det \mathcal{A} + \det \mathcal{B} - 2 \det \mathcal{C}$. The entanglement, can be quantified by the logarithmic negativity, defined as [3],

$$E_N = \max\{0, -ln(2\nu_{\min}\}. \tag{IV.20}$$

Now the optomechanical entanglement, or logarithmic negativity, will be found as a function of two variables simultaneously. The variables that will be used are η (dimensionless multistability

parameter) which will be varied from 0 to 1, and Δ/ω_m (dimensionless normalized effective detuning) which will be varied from 0 to 2. The effective detuning can be calculated from the known variables in Section IV.1. From (IV.15) the multistability parameter can be defined as [3],

$$\eta = 1 + \frac{2G_Q \left|a_s\right|^2}{\omega_m} - \frac{\Delta G^2}{\omega_m \left(\Delta^2 + \kappa^2\right)}. \tag{IV.21}$$

The equation (IV.15) can be simplified to (IV.21). Now that both the multistability parameter and the normalized effective detuning are known, the logarithmic negativity can be calculated. Following the form in [3], each part of the logarithmic negativity can be solved for as the normalized effective detuning ranges from 0 to 2 and the multistability parameter ranges from 0 to 1, as stated above. The entanglement for $G_Q/\omega_m = -3 * 10^{-7}$ is shown in Figure 8, where first the multistability parameter is fixed and the effective detuning is varied, and subsequently their roles are reversed.

This shows that the entanglement parameter is not monotonic in Δ/ω_m and monotonically decreases with η. The resulting entanglement is shown below in Figure 9 for specific values of the quadratic coupling.

As seen in Figure 9 it can be shown when $G_Q/\omega_m = 0$, the optomechanical entanglement is similar in form to the optomechanical entanglement of the cubic from [3]. However, as G_Q/ω_m decreases farther from zero, the resulting optomechanical entanglement is clearly different from the cubic solution. In particular, the threshold of entanglement shifts to the higher effective detuning (Δ/ω_m). To show this difference, the optomechanical entanglement is re-calculated where $G_Q/\omega_m = -3 * 10^5$. Interestingly, when G_Q/ω_m is set to a small positive value, as shown where $G_Q/\omega_m = 3 * 10^{-9}$ the system still results in entanglement. When the effective mechanical frequency (ω_{eff}) goes to zero there is not any resulting entanglement for any effective detuning or multistability parameter. In addition, when $G_Q/\omega_m = 3 * 10^{-7}$ or larger there is not any resulting entanglement.

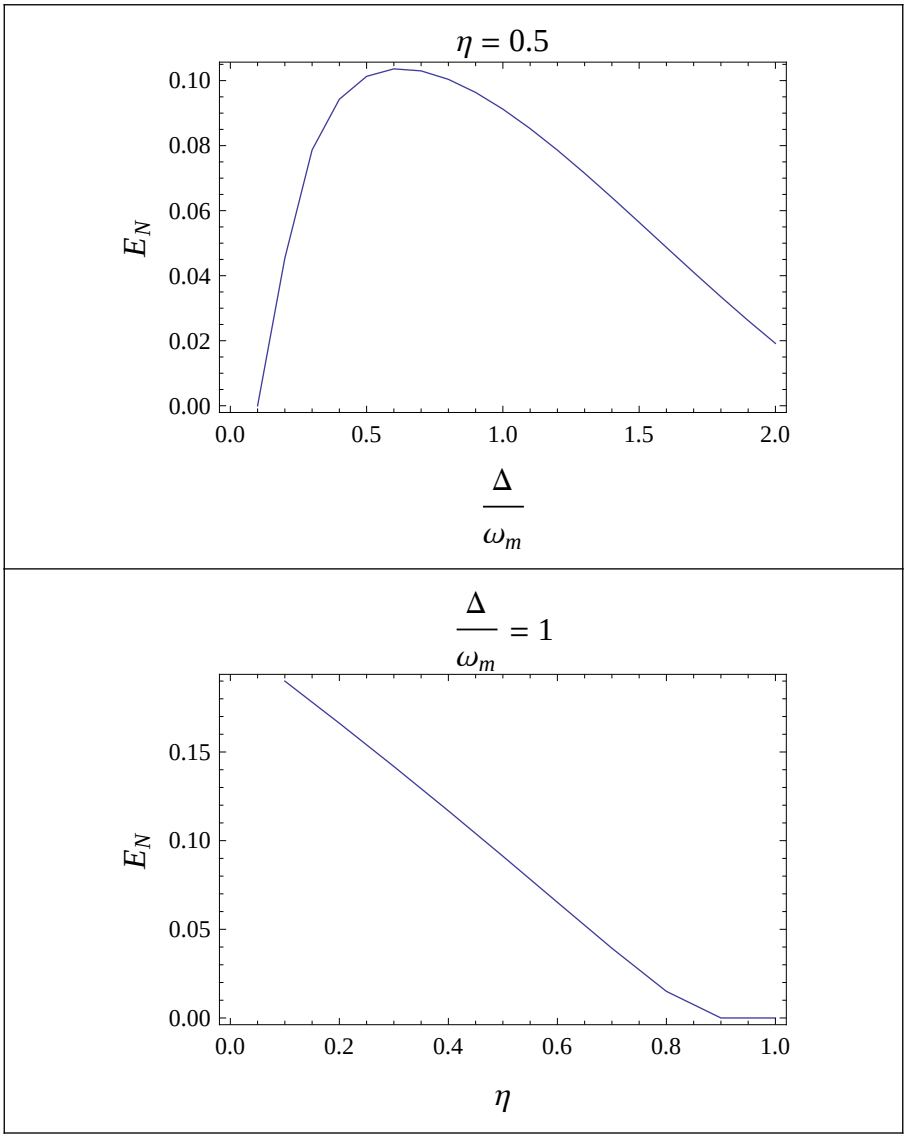

Figure 8: Optomechanical Entanglement, where the parameters used are, $G_Q/\omega_m = -3 * 10^{-7}$, $\kappa/\omega_m = 1.4$, $G_L/\omega_m = 3.4 * 10^{-4}$, $\Delta_\circ/\omega_m = 2.62$, and $\omega_m = 10^7 Hz$, and ambient temperature $T = 0.4K$.

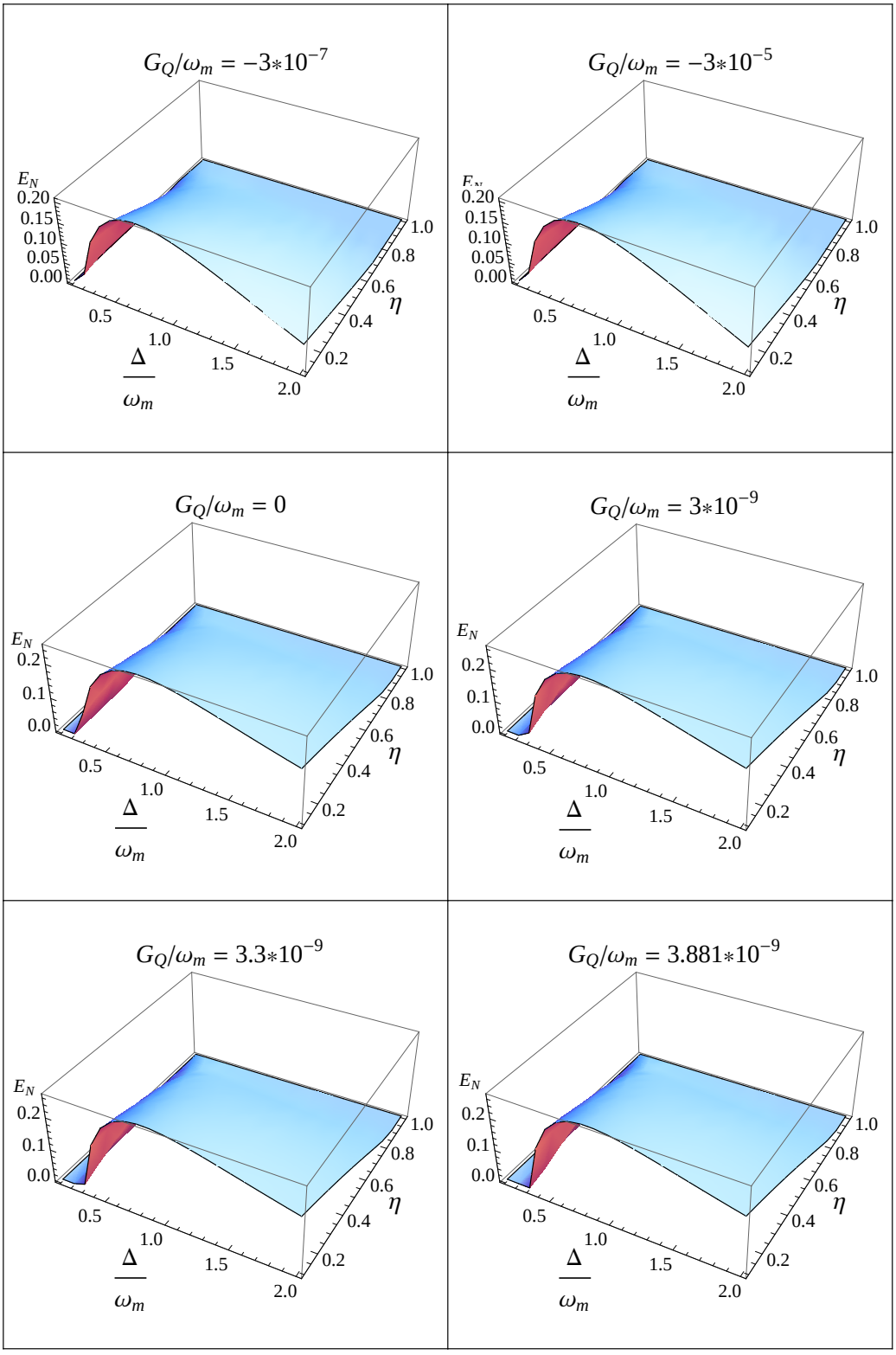

Figure 9: Optomechanical Entanglement, where the parameters used are, $\kappa/\omega_m = 1.4$, $G_L/\omega_m = 3.4 * 10^{-4}$, $\Delta_\circ/\omega_m = 2.62$, and $\omega_m = 10^7 Hz$, and ambient temperature $T = 0.4K$.

V. Conclusion

We have inspected the characteristics of stability and entanglement in an optomechanical system. We have investigated the critical points within the system and used the covariance matrix formulation to extend the investigation of the optomechanical system to characterize the entanglement. By introducing a quadratic coupling into the system, a quintic formulation was achieved. Interestingly, the introduction of the quadratic coupling requires that it be negative, and optimally a small negative number compared to the mechanical frequency, in order to achieve an optomechanical quintic. If however, a positive quadratic coupling is introduced into the system, in which multiple roots are otherwise expected, the roots disappear from the system and an almost linear result is achieved. When a critical point analysis was carried out the locations of such stationary points where found to be on the negative real axis, outside the physical realm of possible results. As expected, when the quadratic coupling was set equal to zero the optomechanical cubic was recovered with corresponding results found in [3]. The effect of adding this quadratic coupling is shown not only in the output of a cubic and quintic equation but also in Figure 2 and Figure 3.

In 1799, Ruffini, and again in 1826, Abel, showed that the solution of the general quintic cannot be formed analytically by radicals in all forms [26]. However, by implementing a quadratic Tschirnhausen transformation, a quartic Tschirnhausen transformation, and a canonical transformation, the general quintic can be reduced to the Bring-Jerrard canonical formulation where the linear constant parameter is in terms of radicals. Though the final solution of the Bring-Jerrard is not solved by radicals, since it may or not be equivalent to one of the special quintics that are solvable by radicals, it is solvable by the hypergeometric formulation. Once the roots are identified, the process of inverting each of the transformations occurs so as to achieve the final set of roots that will satisfy the general quintic. During each inverse transformation the erroneous solutions must be dropped. To do this, each possible solution was substituted into the corresponding quintic formulation and the absolute value of the outputs was taken where the five smallest values identify the corresponding solutions to be used in the next step of inversing the transformations.

As shown in Figure 2 the bistable cubic has two stationary points, it is expected that the quintic would have four stationary points. However, as can be seen in Figure 3 only three stationary points occur within the range shown. It appears that a fourth critical point occurs somewhere outside the range shown in the figure. A numerical inspection shows in fact that this fourth critical point does occur, as is needed, however the critical point is complex and not within the

real regime of I_I or I_T. An analytical investigation of the quintic derivative, shows that for any optomechanical quintic of our form, there is a resulting quintic in the numerator and denominator. This denominator provides the location of the fourth critical point. In addition, the results from [17] further support that the optomechanical quintic system specific to this thesis does in fact have only three stationary points with a fourth critical point pair.

Investigating the fluctuations around the steady-state requires that the covariance matrix be formulated. This formulation comes from inspecting the equations of motion. Once the covariance matrix, is formulated it can be used to inspect the entanglement within the system. To analyze the entanglement, the multistability parameter, which is the distance from the end of the stable branch in a multistable regime, must be formulated. The formulation of the multistability parameter, is based on the Routh-Hurwitz criteria. Using this multistability parameter in conjunction with the normalized effective detuning and ranging both over their respective ranges allows a mesh of the resulting entanglement to be produced, as shown in Figure 9. As expected, when the quadratic coupling is set equal to zero and the bistable cubic is formed. The resulting entanglement is the same as was achieved in [3].

In the future, it would be interesting to investigate the change in stationary and critical points for different optomechanical quintic systems and their resulting entanglement as G_Q is varied. Another direction of investigation may be to inspect the lack of symmetry between the resulting entanglement mesh for negative and positive quadratic coupling constants.

VI. Acknowledgments

I would like to thank my advisor, Dr. Mishkatul Bhattacharya, and my committee Dr. Anthony Harkin, Dr. David Ross and Dr. Nathan Cahill for their support and advice throughout this research. I would like to thank Dr. Michael Kotlarchyk for reading over the thesis. I would like to thank Okechukwu Igbokwe, for his very enlightening discussions. I would also like to thank Eric Sullivan and John Costanzo for their useful discussions.

VII. Appendix

VII.1 Analytic Solution to Quintic

The quintic equation (III.12) can be solved analytically using radicals. However, certain transformations need to be implemented [14]. These transformations are known as the Tschirnhausen transformations and the path that is taken to achieve the final solution of the general quintic equation is discussed below. To save space, simplified versions of the equations derived will be shown. We begin with the equation,

$$AI_T + BI_T\left(C - D\left[\frac{H_1 I_T}{H_2 + H_3 I_T}\right] + E\left[\frac{H_1 I_T}{H_2 + H_3 I_T}\right]^2\right)^2 = I_I.$$

From here the general quintic is formed by dividing by A, setting the equation to zero and then simplifying, assuming $A \neq 0$,

$$x^5 + px^4 + qx^3 + rx^2 + sx + t = 0. \tag{VII.1}$$

VII.1.1 Tschirnhausen Transformations

The general quintic will be the basis for the rest of the derivation and final solution. The quadratic Tschirnhausen transformation will be used to transform the general quintic (IV.1), where p, q, r, s, and t are in terms of A, B, C, D, E, $H1$, $H2$, and $H3$, into the principal quintic. This transformation has the form,

$$y = x^2 + \alpha x + \beta. \tag{VII.2}$$

Using the resultant of the general quintic (IV.1) and the quadratic Tschirnhausen transformation (IV.2) eliminates the variable x to form a new Quintic in y,

$$y^5 + c1y^4 + c2y^3 + c3y^2 + c4y + c5 = 0, \tag{VII.3}$$

where the constants $c1$, $c2$, $c3$, $c4$, and $c5$ are polynomials in terms of p, q, r, s, α, and β. In order to acquire the principal quintic form, the constants $c1$ and $c2$ need to be set equal to zero. Terms $c1$ and $c2$ have the form,

$$c1 = -5\beta - p^2 + \alpha p + 2q, \tag{VII.4}$$

$$c2 = 10\beta^2 + 4\beta p^2 - 4\alpha\beta p - \alpha pq - 2pr + q^2 + \alpha^2 q - 8\beta q + 3\alpha r + 2s. \tag{VII.5}$$

The quantities $c1$ and $c2$ can be set equal to zero by solving for α and β simultaneously. This allows for the principal quintic to be acquired having the form,

$$y^5 + c3y^2 + c4y + c5 = 0. \tag{VII.6}$$

From here, the quartic Tschirnhausen transformation will be used to transform the principal quintic into the Bring-Jerrard quintic,

$$z = y^4 + \mathcal{A}y^3 + y^2\mathcal{B} + \mathcal{C}y + \mathcal{D}. \tag{VII.7}$$

Following similar steps to that of the quadratic transformation, the resultant of the principal quintic (IV.6) and the quartic Tschirnhausen transformation (IV.7) eliminates the variable y to form a new quintic in z,

$$z^5 + C1z^4 + C2z^3 + C3z^2 + C4z + C5 = 0, \tag{VII.8}$$

where the constants $C1$, $C2$, $C3$, $C4$, and $C5$ are in terms of $c3$, $c4$, $c5$, $\mathcal{A}$, $\mathcal{B}$, $\mathcal{C}$, and $\mathcal{D}$. Similarly, $C1$, $C2$, and $C3$ need to be set to zero in order to achieve the Bring-Jerrard quintic form. Terms $C1$ and $C2$ have the form,

$$C1 = 3\mathcal{A}c3 + 4c4 - 5\mathcal{D}. \tag{VII.9}$$

$$\begin{aligned} C2 =& 3\mathcal{A}^2c3^2 - 3c3^2\mathcal{B} - 12\mathcal{A}c3\mathcal{D} + 5\mathcal{A}c3c4 + \mathcal{C}(3c3\mathcal{B} + 4\mathcal{A}c4 + 5c5) - 4c3c5 + 6c4^2 \\ & - 16c4\mathcal{D} + 2c4\mathcal{B}^2 + 5\mathcal{A}c5\mathcal{B} + 10\mathcal{D}^2. \end{aligned} \tag{VII.10}$$

Setting $C1 = 0$ and solving for $\mathcal{D}$ results in,

$$\mathcal{D} = \frac{1}{5}(3\mathcal{A}c3 + 4c4). \tag{VII.11}$$

Allowing the variable constant $\mathcal{C}$ to be a "free" variable by eliminating it from $C2$ can be done by solving for $\mathcal{B}$ from letting,

$$3c3\mathcal{B} + 4\mathcal{A}c4 + 5c5 = 0. \tag{VII.12}$$

Solving for $\mathcal{B}$ results in,

$$\mathcal{B} = \frac{-4\mathcal{A}c4 - 5c5}{3c3}. \tag{VII.13}$$

Now that $\mathcal{B}$, and $\mathcal{D}$ have been solved for the constant $C2$ can be set equal to zero and a quadratic equation in $\mathcal{A}$ is formed,

$$\begin{aligned} & \mathcal{A}^2\left(-27c3^4 - 300c3c4c5 + 160c4^3\right) + \mathcal{A}\left(-27c3^3c4 - 375c3c5^2 + 400c4^2c5\right) + 45c3^3c5 \\ & - 18c3^2c4^2 + 250c4c5^2 = 0. \end{aligned} \tag{VII.14}$$

Solving for $\mathcal{A}$ will now allow the variable constant $C3$ to be set equal to zero and the resulting cubic in $\mathcal{C}$ to be solved for,

$$\begin{aligned}
&\mathcal{C}^3 c3 + \mathcal{C}^2\left(-3c3^2 + 4c4\mathcal{B} + 5\mathcal{A}c5\right) + \mathcal{C}\left(3c3^3 + 3\mathcal{A}c3^2\mathcal{B} + 5\mathcal{A}^2c3c4 - 2c3c4\mathcal{B} - \mathcal{A}c3c5 - 9c3\mathcal{D}\mathcal{B}\right.\\
&\qquad\left. + 8\mathcal{A}c4^2 - 12\mathcal{A}c4\mathcal{D} + 11c4c5 - 15c5\mathcal{D} + 5c5\mathcal{B}^2\right) + 18\mathcal{A}c3\mathcal{D}^2 + \mathcal{A}c3c4^2 - 15\mathcal{A}c3c4\mathcal{D}\\
&- \mathcal{A}c3c4\mathcal{B}^2 - 8c3c4c5 + 7\mathcal{A}^2c3c5\mathcal{B} + 12c3c5\mathcal{D} - 8c3c5\mathcal{B}^2 + 4c4^3 - 4\mathcal{A}^2c4^2\mathcal{B} - 18c4^2\mathcal{D} + 4c4^2\mathcal{B}^2\\
&- 3\mathcal{A}^3c4c5 + 2\mathcal{A}c4c5\mathcal{B} + 24c4\mathcal{D}^2 - 6c4\mathcal{D}\mathcal{B}^2 - 5\mathcal{A}^2c5^2 - 5c5^2\mathcal{B} - 15\mathcal{A}c5\mathcal{D}\mathcal{B} - 10\mathcal{D}^3 - c3^4\\
&+ \mathcal{A}^3c3^3 - 3\mathcal{A}c3^3\mathcal{B} - 9\mathcal{A}^2c3^2\mathcal{D} + \mathcal{A}^2c3^2c4 - 2c3^2c4\mathcal{B} - \mathcal{A}c3^2c5 - c3^2\mathcal{B}^3 + 9c3^2\mathcal{D}\mathcal{B} = 0.
\end{aligned} \tag{VII.15}$$

Since the resulting radical solution of $\mathcal{C}$ is large, the solution will not be shown here. Now that the variables $\mathcal{A}$, $\mathcal{B}$, and $\mathcal{C}$ have been solved for in such a way as to allow $C1$, $C2$, and $C3$ to be set equal to zero. The Bring-Jerrard quintic equation can now be written and has the form,

$$z^5 + C4z + C5 = 0. \tag{VII.16}$$

VII.1.2 Canonical Transformation and Hypergeometric Equations

Finally in order to solve this equation the Bring-Jerrard quintic needs to be transformed into the Bring-Jerrard normal form, also referred to as the Bring-Jerrard canonical form [27]. This is done by doing a canonical transformation on the Bring-Jerrard quintic to transform it it into the Bring-Jerrard normal form. The linear transformation has the form,

$$t = (-C4^{\frac{1}{\Delta}})z, \tag{VII.17}$$

where $\Delta = n - 1$, and n is equal to the order of the equation, therefore $\Delta = 4$. Applying the canonical transformation (IV.17) to the Bring-Jerrard quintic (IV.16), results in the Bring-Jerrard normal form,

$$t^5 - t + \frac{C5}{(-C4)^{\frac{5}{4}}} = 0. \tag{VII.18}$$

Now that the Bring-Jerrard normal form has been found, it can be solved using hypergeometric equations [28]. To do this first the constant Ξ needs to be solved for using the following equation,

$$\Xi = \left(\frac{b}{4}\right)^4 \left(\frac{5}{g}\right)^5, \tag{VII.19}$$

where $g = -1$ and $b = -\frac{\text{C5}}{(-\text{C4})^{\frac{5}{4}}}$.

If $|\Xi| < 1$ the hypergeometric functions are as follows,

$$\begin{aligned}
F_0 &= {}_4F_3\left(-\frac{1}{20}, \frac{3}{20}, \frac{7}{20}, \frac{11}{20}; \frac{1}{4}, \frac{2}{4}, \frac{3}{4}; \xi\right), \\
F_1 &= {}_4F_3\left(\frac{1}{5}, \frac{2}{5}, \frac{3}{5}, \frac{4}{5}; \frac{2}{4}, \frac{3}{4}, \frac{5}{4}; \xi\right), \\
F_2 &= {}_4F_3\left(\frac{9}{20}, \frac{13}{20}, \frac{17}{20}, \frac{21}{20}; \frac{3}{4}, \frac{5}{4}, \frac{6}{4}; \xi\right), \\
F_3 &= {}_4F_3\left(\frac{7}{10}, \frac{9}{10}, \frac{11}{10}, \frac{13}{10}; \frac{5}{4}, \frac{6}{4}, \frac{7}{4}; \xi\right),
\end{aligned} \tag{VII.20}$$

the solutions to our quintic are,

$$\begin{aligned}
t_1 &= -\frac{5b^3F_3}{2^5} + \frac{5ib^2F_2}{2^5} + \frac{bF_1}{4} + iF_0, \\
t_2 &= \frac{5b^3F_3}{2^5} + \frac{5b^2F_2}{2^5} + \frac{bF_1}{4} - F_0, \\
t_3 &= -\frac{5b^3F_3}{2^5} - \frac{5ib^2F_2}{2^5} + \frac{bF_1}{4} - iF_0, \\
t_4 &= \frac{5b^3F_3}{2^5} - \frac{5b^2F_2}{2^5} + \frac{bF_1}{4} + F_0, \\
t_5 &= -bF_1.
\end{aligned} \tag{VII.21}$$

If $|\Xi| > 1$, the hypergeometric functions are as follows,

$$\begin{aligned}
\psi_0 &= {}_4F_3\left(-\frac{1}{20}, \frac{7}{20}, \frac{9}{20}, \frac{1}{5}; \frac{4}{5}, \frac{3}{5}, \frac{2}{5}; \frac{1}{\xi}\right), \\
\psi_1 &= {}_4F_3\left(\frac{3}{20}, \frac{9}{10}, \frac{13}{20}, \frac{2}{5}; \frac{6}{5}, \frac{4}{5}, \frac{3}{5}; \frac{1}{\xi}\right), \\
\psi_2 &= {}_4F_3\left(\frac{7}{20}, \frac{11}{20}, \frac{17}{20}, \frac{3}{5}; \frac{7}{5}, \frac{6}{5}, \frac{4}{5}; \frac{1}{\xi}\right), \\
\psi_3 &= {}_4F_3\left(\frac{11}{20}, \frac{13}{10}, \frac{21}{20}, \frac{4}{5}; \frac{6}{5}, \frac{7}{5}, \frac{6}{5}; \frac{1}{\xi}\right),
\end{aligned} \tag{VII.22}$$

this results in the solutions,

$$\begin{aligned}
t_1 &= \frac{1}{125}b^{-\frac{11}{5}}\psi_3\epsilon^4 - \frac{1}{25}b^{-\frac{7}{5}}\psi_2\epsilon^3 + \frac{1}{5}b^{-\frac{3}{5}}\psi_1\epsilon^2 + b^{\frac{1}{5}}\psi_0\epsilon, \\
t_2 &= \frac{1}{5}b^{-\frac{3}{5}}\psi_1\epsilon^4 + \frac{1}{125}b^{-\frac{11}{5}}\psi_3\epsilon^3 - \frac{1}{25}b^{-\frac{7}{5}}\psi_2\epsilon + b^{\frac{1}{5}}\psi_0\epsilon^2, \\
t_3 &= -\frac{1}{25}b^{-\frac{7}{5}}\psi_2\epsilon^4 + \frac{1}{125}b^{-\frac{11}{5}}\psi_3\epsilon^2 + \frac{1}{5}b^{-\frac{3}{5}}\psi_1\epsilon + b^{\frac{1}{5}}\psi_0\epsilon^3, \\
t_4 &= \frac{1}{5}b^{-\frac{3}{5}}\psi_1\epsilon^3 - \frac{1}{25}b^{-\frac{7}{5}}\psi_2\epsilon^2 + \frac{1}{125}b^{-\frac{11}{5}}\psi_3\epsilon + b^{\frac{1}{5}}\psi_0\epsilon^4, \\
t_5 &= \frac{1}{5}b^{-\frac{3}{5}}\psi_1 - \frac{1}{25}b^{-\frac{7}{5}}\psi_2 + \frac{1}{125}b^{-\frac{11}{5}}\psi_3 + b^{\frac{1}{5}}\psi_0,
\end{aligned} \tag{VII.23}$$

where ϵ is a primitive root of $\epsilon^5 = 1$, and for simplicity $\epsilon = e^{\frac{2\pi i}{5}}$ is chosen to solve the roots.

VII.1.3 Inverse Transformations and Solution

With the solutions to the Bring-Jerrard normal form solved for, the solutions can be used to invert each of the transformations taken to achieve the Bring-Jerrard normal form and ultimately solve for the general quintic equation.

The first inverse transformation is straightforward in that it is a linear transformation. Therefore, solving for z is done using (IV.15),

$$z = -\mathrm{C}4^{\frac{1}{4}} t_i,$$

where i ranges from 1 to 5 resulting in t_i being the solution of each root found in either (IV.19) or (IV.21). Since there are five solutions of t, the output consists of five solutions of z.

The process of solving the quintic with Tschirnhausen transformations creates numerical error within the analytical calculations in the form of complex numbers that should be strictly real. Due to the small error within each transformation, the error compounds on itself, in addition, spurious solutions arise. Thus after doing each inverse transformation the erroneous solutions must be dropped. For this first inverse transformation the imaginary parts of each z solution are dropped if the imaginary part is less than 10^{-10}. Once this step is done the next inverse transformation can be done to solve for y using (IV.6),

$$z = y^4 + \mathcal{A}y^3 + y^2\mathcal{B} + \mathcal{C}y + \mathcal{D}.$$

Finding and dropping the erroneous solutions within the next two steps of inversing the solutions becomes a bit more complicated. In order to drop the erroneous solutions, each solution of y needs to be substituted into a variation of (IV.5). This variation is as follows,

$$y^5 + c3y^2 + c4y + c5.$$

There are only five solutions of y that will produce sensible, closest to zero, solutions. In order to determine the five solutions or roots of y from the 20 that were calculated, once each y_i, where i ranges from 1 to 20, is plugged into the above variation of (IV.5) the absolute value of each result needs to then be taken. The sensible solutions are those solutions that correlate to the first five, or smallest, absolute values, the remaining solutions are erroneous. These five solutions will be used in the next step of inversing the Tschirnhausen transformations. Following the procedure from the previous step the inverse transformation to solve x can be done using (IV.2),

$$y = x^2 + \alpha x + \beta.$$

Again each solution of x needs to be substituted into a variation of the general quintic equation (IV.1) where the zero is dropped,

$$x^5 + px^4 + qx^3 + rx^2 + sx + t.$$

In this case there are only 10 solutions of x that need to be tested. Similarly, the sensible solutions are those solutions of x_i that correlate to the first five, or smallest, absolute values, where the remaining solutions are erroneous. However, there is one more step that needs to be carried out before the five solutions of x that where just found be accepted as the final solution to the general quintic. As in the first step of inversing the canonical and Tschirnhausen transformations, the imaginary parts that are sufficiently small within each solution of x need to be dropped as done above with the solutions of z. However, in this step the imaginary part is dropped if it is less than 0.1. This will result in the five true roots or solutions of x that solve the general quintic and therefore the optomechanical quintic since $x = I_T$.

The analytical solution of the optomechanical quintic using the Tschirnhausen transformations, shown by dots, and the corresponding numerical quintic, shown by x, is shown in Figure 10. In the graph a step size of 1 is used for I_I. A larger step size is used due to the error, mentioned above, that results in doing the Tschirnhausen transformations. The parameters used the previous two figures differ from the parameters used throughout this thesis because when solving the quintic equation using the Tschirnhausen transformations erroneous outputs where given. These erroneous outputs were achieved due to the automation of solving for the roots. If the inverse transformations are done manually the erroneous solutions can be identified. However, this requires a large amount of time based on the range. For this reason a simpler system was solved and displayed. In comparing the roots from Figure 8, an obviously erroneous point is removed from the system, after which a Percent Error of 0.0148501 is found. This shows that the Tschirnhausen transformations paired with the canonical transformation and hypergeometric equations do allow for the system to be solved for with a high level of accuracy.

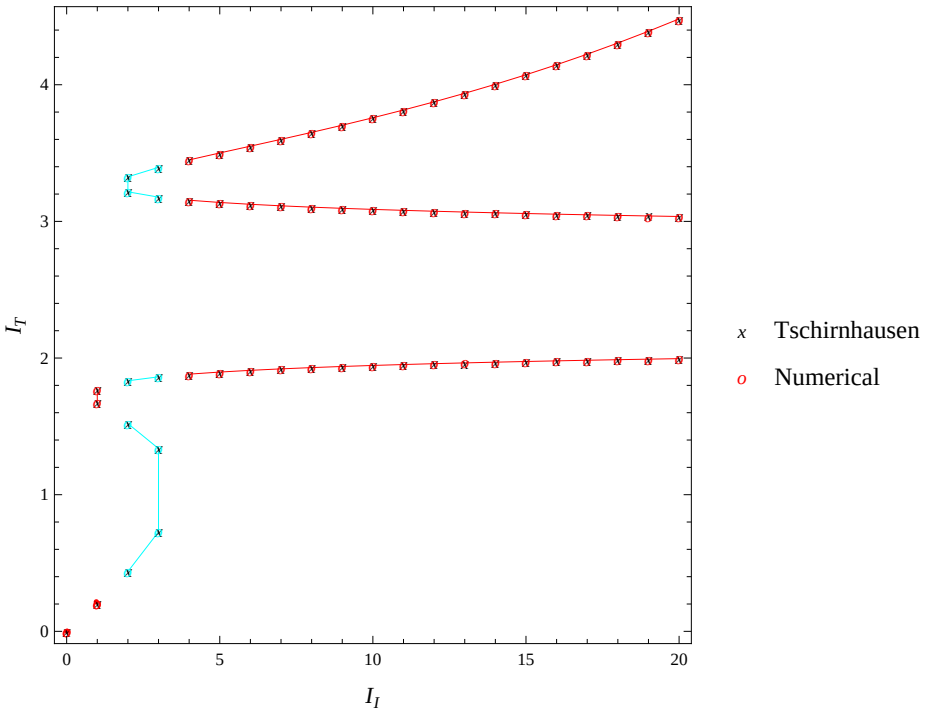

Figure 10: Quintic using Tschirnhausen Transformations and Hypergeometric Equations, where I_I and I_T are dimensionless. The parameters used are, $\kappa/\omega_m = 1/2$, $G_L/\omega_m = 1/4$, $G_Q/\omega_m = -1/10$, $\Delta_\circ/\omega_m = 1.5$, and $\omega_m = 10^7 Hz$. The first point at $(0,0)$ has a single root. The segments in red represents three real roots and the segments in cyan represent five real roots.

VIII. Bibliography

References

[1] M. Aspelmeyer, T.J. Kippenberg, and F. Marquardt (2013). Cavity Optomechanics. *arXiv preprint*, arXiv:1303.0733 [cond-mat.mes-hall].

[2] E. Abraham, and S.D. Smith (1982). Optical bistability and related devices. *Reports on Progress in Physics*, 45.8: 815.

[3] R. Ghobadi, A.R. Bahrampour, and C. Simon (2011). Quantum Optomechanics in the Bistable Regime. *Physical Review*, A 84.3, 033846.

[4] P. Meystre, and M. Sargent (2007). Elements of Quantum Optics. Springer.

[5] J.D. Thompson, B.M. Zwickl, A.M. Jayich, F. Marquardt, S.M. Girvin, and J.G.E Harris (2008). Strong Dispersive Coupling of a High-Finesse Cavity to a Micromechanical Membrane. *Nature*, 452.7183: 72-75.

[6] V. Giovannetti, and D. Vitali (2001). Phase-noise measurement in a cavity with a movable mirror undergoing quantum Brownian motion. *Physical Review*, A 63.2, 023812.

[7] D.J. Griffiths (2004). Introduction to quantum mechanics. 2nd. Pearson Prentice Hall.

[8] C. Gardiner, and P. Zoller (2004). Quantum noise: a handbook of Markovian and non-Markovian quantum stochastic methods with applications to quantum optics. *Springer*, Vol. 56.

[9] C. Genes, D. Vitali, P. Tombesi, S. Gigan, and M. Aspelmeyer (2008). Ground-state cooling of a micromechanical oscillator: Comparing cold damping and cavity-assisted cooling schemes. *Physical Review*, A 77.3, 033804.

[10] J.B. Hertzberg, T. Rocheleau, T. Ndukum, M. Savva, A.A. Clerk, and K.C. Schwab (2009). Back-action-evading measurements of nanomechanical motion. *Nature Physics*, 6 no. 3 (2009): 213-217.

[11] I.D. Rukhlenko, M. Premaratne, and G.P. Agrawal (2009). Analytical study of optical bistability in silicon-waveguide resonators. *Optics express*, 17, no. 24: 22124-22137.

[12] J. Jiang, and J. Shi (2010). Bistability dynamics in structured ecological models. *Spatial Ecology*, Taylor and Francis, New Jersey: 33-62.

[13] L. Perko (2001). Differential Equations and Dynamical Systems (Texts in Applied Mathematics). *Springer*, 3rd edition.

[14] T. Piezas III. A New Way To Derive The Bring-Jerrard Quintic In Radicals.

[15] V.S. Adamchik, and D.J. Jeffrey (2003). Polynomial transformations of tschirnhaus, bring and jerrard. *ACM SIGSAM Bulletin*, 37.3 : 90-94.

[16] R.J. Drociuk (2000). On the complete solution to the most general fifth degree polynomial. *arXiv preprint* math/0005026 .

[17] T.W. Chaundy (1933). On the Number of Real Roots of a Quintic Equation.

[18] L. Shenping, R. Pons, and G.T. Orriols (1994). Analysis on the stability and dynamic response of the laser with a bistable mirror. *Volga Laser Tour'93*, International Society for Optics and Photonics.

[19] C. Gardiner, and P. Zoller (2004). Quantum noise: a handbook of Markovian and non-Markovian quantum stochastic methods with applications to quantum optics. *Springer*, Vol. 56.

[20] S. Shahidani, M.H. Naderi, M. Soltanolkotabi, and S. Barzanjeh (2013). Steady state entanglement, cooling, and tristability in a nonlinear optomechanical cavity. *arXiv preprint*, arXiv:1310.6251.

[21] E.X. DeJesus, and C. Kaufman (1987). Routh-Hurwitz criterion in the examination of eigenvalues of a system of nonlinear ordinary differential equations. *Physical Review*, A 35.12, 5288.

[22] A. Mari, and J. Eisert (2009). Gently modulating optomechanical systems. *Physical Review Letters*, 103.21, 213603.

[23] M. Bhattacharya, P-L. Giscard, and P. Meystre (2008). Entanglement of a Laguerre-Gaussian cavity mode with a rotating mirror. *Physical Review*, A 77.1, 013827.

[24] C. Biancofiore, M. Karuza, M. Galassi, R. Natali, P. Tombesi, G. Di Giuseppe, and D. Vitali (2011). Quantum dynamics of an optical cavity coupled to a thin semitransparent membrane: Effect of membrane absorption. *Physical Review*, A 84.3, 033814.

[25] A. Mari, and J. Eisert (2009). Gently modulating optomechanical systems. *Physical Review Letters*, 103.21, 213603.

[26] N. Jacobson (2009). Basic Algebra I. *Dover Publications*, Second Edition.

[27] Poster: Solving the Quintic, Wolfram Research, Inc. Champaign, IL, 1995. http://library.wolfram.com/examples/quintic/.

[28] R. Birkeland. On the Solutions of Quintic Equations. University of Oslo, Oslo, Norway. http://www.mathunion.org/ICM/ICM1924.1/Main/icm1924.1.0387.0398.ocr.pdf